

Structural insight into the evolutionary and pharmacologic homology of glutamate carboxypeptidases II and III

Klara Hloučová^{1,2}, Cyril Barinka³, Jan Konvalinka^{1,2} and Jacek Lubkowski³

¹ Gilead Sciences and IOCB Research Centre, Institute of Organic Chemistry and Biochemistry, Academy of Sciences of the Czech Republic, Prague, Czech Republic

² Department of Biochemistry, Faculty of Natural Science, Charles University, Prague, Czech Republic

³ Center for Cancer Research, National Cancer Institute at Frederick, MD, USA

Keywords

GCPIII; M28 family; metallopeptidase; NAALADase II; prostate specific membrane antigen

Correspondence

J. Lubkowski or J. Konvalinka,
Macromolecular Crystallography Laboratory,
539 Boyles Street, National Cancer Institute
at Frederick, Frederick, MD 21702, USA;
Institute of Organic Chemistry and
Biochemistry, Gilead Sciences & IOCB
Research Center, Academy of Sciences of
the Czech Republic, Flemingovo nám. 2,
166 10 Praha 6, Czech Republic
Fax: +301 846 7517; +420 220 183 578
Tel: +301 846 5494; +420 220 183 218
E-mail: jacek@ncifcrf.gov;
konval@uochb.cas.cz

Database

The atomic coordinates of the structures described in the present study, together with the experimental structure factor amplitudes, have been deposited in the RCSB Protein Data Bank with accession codes: 3FF3 (glutamate complex), 3FEE (the complex with QA), 3FED (the complex with EPE) and 3FEC (the 'pseudo-unliganded' state)

(Received 27 April 2009, revised 3 June 2009, accepted 12 June 2009)

doi:10.1111/j.1742-4658.2009.07152.x

Glutamate carboxypeptidase III (GCPIII) is a metalloenzyme that belongs to the transferrin receptor/glutamate carboxypeptidase II (GCPII; EC 3.4.17.21) superfamily. GCPIII has been studied mainly because of its evolutionary relationship to GCPII, an enzyme involved in a variety of neuro-pathologies and malignancies, such as glutamatergic neurotoxicity and prostate cancer. Given the potential functional and pharmacological overlap between GCPIII and GCPII, studies addressing the structural and physiological properties of GCPIII are crucial for obtaining a deeper understanding of the GCPII/GCPIII system. In the present study, we report high-resolution crystal structures of the human GCPIII ectodomain in a 'pseudo-unliganded' state and in a complex with: (a) L-glutamate (a product of hydrolysis); (b) a phosphapeptide transition state mimetic, namely (2*S*,3'*S*)-{[(3'-amino-3'-carboxy-propyl)-hydroxyphosphinoyl]methyl}-pentanedioic acid; and (c) quisqualic acid, a glutamate biostere. Our data reveal the overall fold and quaternary arrangement of the GCPIII molecule, define the architecture of the GCPIII substrate-binding cavity, and offer an experimental evidence for the presence of Zn²⁺ ions in the bimetallic active site. Furthermore, the structures allow us to detail interactions between the enzyme and its ligands and to characterize the functional flexibility of GCPIII, which is essential for substrate recognition. A comparison of these GCPIII structures with the equivalent GCPII complexes reveals differences in the organization of specificity pockets, in surface charge distribution, and in the occupancy of the co-catalytic zinc sites. The data presented here provide information that should prove to be essential for the structurally-aided design of GCPIII-specific inhibitors and might comprise guidelines for future comparative GCPII/GCPIII studies.

Abbreviations

EPE, (2*S*,3'*S*)-{[(3'-amino-3'-carboxy-propyl)-hydroxyphosphinoyl]methyl}-pentanedioic acid; GCPIII (III), glutamate carboxypeptidase III (II); NAAG, *N*-acetyl-L-aspartyl-L-glutamate; NAG, *N*-acetylglucosamine; PDB, Protein Data Bank; PPII, polyproline type II; QA, quisqualic acid; rhGCPII, recombinant human glutamate carboxypeptidase II (extracellular domain; residues 44–750); rhGCPIII, recombinant human glutamate carboxypeptidase III (extracellular domain; residues 36–740); TfR, transferrin receptor.

Introduction

Glutamate carboxypeptidase III (GCPIII), a membrane-bound metalloenzyme, belongs to the MEROPS M28 peptidase family (<http://merops.sanger.ac.uk/>), which encompasses a variety of proteins with considerable functional diversity, including peptidases (e.g. aminopeptidases, GCPII, GCPIII and plasma glutamate carboxypeptidase), receptor proteins [transferrin receptors (TfRs)], acyltransferases (glutaminyl cyclases), signaling molecules (nicalin), as well as proteins with as yet unknown functions [1,2]. Currently, the physiological role and tissue distribution of GCPIII are not known in detail. GCPIII mRNA expression has been observed in a variety of human and mouse tissues, with the strongest signals being detected in the testis, ovary, spleen and discrete brain areas [3,4]. Because of the lack of GCPIII-specific antibodies, the expression pattern of GCPIII at the protein level remains unknown.

By contrast to the relative lack of experimental data for GCPIII, there are numerous reports regarding its closest homolog, GCPII (EC 3.4.17.21). GCPII, also known as NAALADase or prostate specific membrane antigen [5,6], is a membrane-bound metallopeptidase that is expressed in numerous human tissues, including the nervous system, small intestine and prostate [7–9]. By virtue of its involvement in glutamatergic neurotransmission [10], inhibition of the GCPII enzymatic activity has been shown to be neuroprotective in multiple preclinical models of various pathophysiological conditions [11]. Furthermore, even though the physiological function of the enzyme in the prostate is poorly understood, up-regulation of GCPII expression in prostate carcinoma makes it a target for prostate cancer imaging and therapy [12–17]. In addition to its role in peptide hydrolysis, GCPII has been found to affect the cell cycle [18] and to modulate integrin signaling [19]. Additionally, it might function as a receptor for as yet unidentified ligand(s) [20]. Taking into account the non-enzymatic functions attributable to GCPII, it may be considered as a representative of a growing family of ‘moonlighting’ enzymes [21,22].

The physiological significance of GCPIII has been addressed only indirectly using knockout mouse models deficient in the gene encoding GCPII, which shares 67% identity with GCPIII at the amino acid level [23,24]. Whereas Tsai *et al.* [24] found GCPII to be crucial for the survival of mouse embryos, the results obtained by Bacich *et al.* [23] suggest that GCPIII can compensate for the missing GCPII protein (at least in part), including hydrolysis of *N*-acetyl-aspartyl-glutamate (NAAG), the natural dipeptidic substrate, in

mouse brain [23]. In a study using a recombinant protein expressed in insect cells, we confirmed that GCPIII is capable of hydrolyzing NAAG *in vitro*, and we provided a direct comparison of the biochemical and pharmacological profiles of GCPII and GCPIII. Although we observed differences in pH and salt concentration dependence and noted that the enzymes have distinct substrate specificities, their inhibitory profiles were quite similar [25].

X-ray crystallographic studies revealed structural similarity between GCPII and the TfR [26,27]. The GCPII ectodomain consists of three distinct domains, namely protease, apical and dimerization (or helical), and all three domains are involved in substrate binding [27–29]. Substrate recognition by GCPII is associated with an induced-fit repositioning of the flexible loop around Lys699 (the ‘glutarate sensor’). The conformation of the ‘glutarate sensor’ depends on occupancy of the S1’ specificity pocket by glutamate or glutamate-like residues [27,30]. The binuclear active site of GCPII harbors two Zn²⁺ ions that are bridged near-symmetrically by a hydroxide anion [31], with the distance between the zinc ions varying depending on the presence and characteristics of an active site ligand [27,30]. The S1 pocket of GCPII is defined primarily by the side chains of three closely spaced Arg residues (534, 536 and 463). Whereas the position of the Arg534 side chain is virtually constant in all reported GCPII structures, the side chains of Arg536 and Arg463 accommodate variable conformations [29]. The flexibility of the S1 arginines is considered to regulate GCPII affinity towards different inhibitors and modulate GCPII substrate specificity [29,30,32]. The substrate-binding pocket of GCPII is shielded from the external space by the ‘entrance lid’, a flexible segment comprising residues Trp541–Gly548. The ‘entrance lid’ is hinged by Asn540/Trp541 and Gly548 at its N- and C-terminus, respectively, and the transition between open and closed conformations appears to depend on the presence of a ligand molecule in the substrate-binding pocket [29].

Even though GCPIII is still not well-characterized and its particular physiological roles remain elusive, a detailed understanding of the structural properties of this protein is very important. As noted above, GCPII, the closest homolog of GCPIII, is currently a target of intensive drug development for the treatment of prostate cancer, amongst other areas [33]. Because of their extensive similarity, GCPII and GCPIII display a range of overlapping activities *in vitro*, yet even the presently available data indicate subtle differences

between the substrate preferences or inhibitor susceptibilities of both enzymes. The rational development of potent agents that would inhibit their glutamate carboxypeptidase activity has to account for the properties of both GCPII and GCPIII. Thus, structural data for the latter enzyme and its complexes with various ligands should prove immediately useful, even though detailed biological and physiological data might become available only later.

In the present study, we report a comprehensive structural analysis of several functional complexes of recombinant human GCPIII (rhGCPIII), solved and refined at resolutions in the range 1.29–1.56 Å. The structures presented include complexes of GCPIII and (a) (2*S*,3'*S*)-{[(3'-amino-3'-carboxy-propyl)-hydroxy phosphinoyl]methyl}-pentanedioic acid (EPE), a phosphopeptide transition state analog of glutamyl-glutamate (rhGCPIII/EPE); (b) L-glutamate, a product of NAAG hydrolysis (rhGCPIII/Glu); and (c) 2-amino-3-(3,5-dioxo[1,2,4]oxadiazolidin-2-yl)propionic acid (quisqualic acid; QA), a glutamate-like inhibitor of GCPIII (rhGCPIII/QA; Table 1). The fourth structure is referred to here as a 'pseudo-unliganded' GCPIII because no ligands were added to the protein prior to crystallization. However, we found that molecules of L-glutamic acid (binding as in rhGCPIII/Glu) and Mops occupy the substrate-binding cavity of 'pseudo-

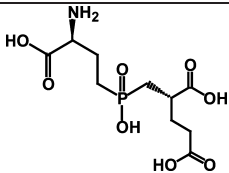
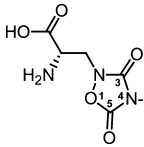
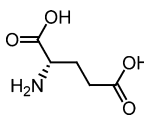
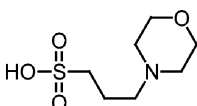
unliganded' rhGCPIII. Crystal structures of analogous complexes have been reported recently for GCPII, allowing direct comparison between the two enzymes [27–29].

Results

Overall structure, dimerization interface and N-glycosylation sites

The rhGCPIII polypeptide chain folds into three structural domains, which are analogous to the three domains of GCPII [27]: a protease domain (amino acids 46–106 and 342–580), an apical domain (amino acids 107–341) and a helical domain (amino acids 581–740). The overall structures of both proteins are quite similar, with rmsd values between the equivalent C α -atoms of GCPIII and GCPII in the range 0.6–1.0 Å. The fold of the protease domain resembles a typical M28 peptidase, with a central motif consisting of seven β -strands flanked by eleven α -helices. The apical domain (or the protease associated domain) is inserted into the protease domain and features a (3 + 4)-stranded β -sandwich flanked by four α -helices. The principal motif of the helical domain (or transferrin-like dimerization domain) is a four α -helix bundle (Fig. 1).

Table 1. Inhibition constants of substrate/product analogs used for co-crystallization with rhGCPIII. ND, not determined.

Inhibitor	Molecular structure	GCPII K_i /nM	GCPIII K_i /nM
EPE		12.9 \pm 3.9 ^a	34.6 \pm 5.7
QA		1020 \pm 110	230 \pm 24
L-Glu		428 \times 10 ^{3b}	270 \times 10 ³ \pm 124 \times 10 ³
MOPS		ND	ND

^a Taken from Barinka *et al.* [29]. ^b Taken from Barinka *et al.* [28].

In the crystal, one monomer of GCPIII is present in the asymmetric unit, with a dimer formed by crystallographic symmetry. The relevance of the dimer can be derived by comparison with the related GCPII and TfR as well as by analysis of the crystallographic contacts within GCPIII crystals. The total surface area for the interface buried upon dimerization is 2390 Å², and the putative dimerization interface mostly involves interactions between residues of the helical domain of one monomer and residues of the protease and apical domains of the second monomer (Fig. 1B). The conserved calcium-binding residues near the putative monomer–monomer interface likely contribute to GCPIII folding and dimerization by (a) stabilizing the loop Tyr262-Phe269, which participates in dimerization contacts, and (b) allowing proper positioning of the protease and apical domains via simultaneous engagement of residues adjacent to Ca²⁺, as described for GCPII [27].

Predictions suggest seven potential N-glycosylation sites per GCPIII molecule. The interpretable electron density peaks were observed for four of these sites (Asn111, Asn185, Asn449 and Asn628) and, for each of them, one or two *N*-acetylglucosamine (NAG) molecules were modeled (Fig. 1B,C). Overall, GCPIII molecule is thus less heavily N-glycosylated than GCPII, with seven out of ten potential glycosylations being observed in the structures solved [28,29]. Moreover, no electron density peaks were found for the mannose units of the N-linked oligosaccharides, probably as a result of the increased flexibility of the more distal carbohydrate parts. Similar to previously reported findings for GCPII [27], N-glycosylation of Asn628 appears to contribute to the stabilization of GCPIII dimers through interactions between Asn628-NAG₂ of one monomer and the side chain of Glu266 of the apical domain of the second monomer.

The binuclear metal center

Electron density maps reveal the presence of two metal ions in the active site of GCPIII. Because of the high level of homology between GCPIII and GCPII, it is reasonable to assume that both metal sites are occupied by Zn²⁺ ions. However, the identity of the metal ions became questionable even during the early stages of structural refinement, giving way to at least two possibilities: partial occupancy of Zn²⁺ sites or, alternatively, the presence of different (most likely lighter) metal ions such as Mn²⁺ or Co²⁺. To elucidate this ambiguity, we performed X-ray fluorescence scan analysis of the rhGCPIII/EPE complex (data not shown). Furthermore, we calculated the anomalous electron

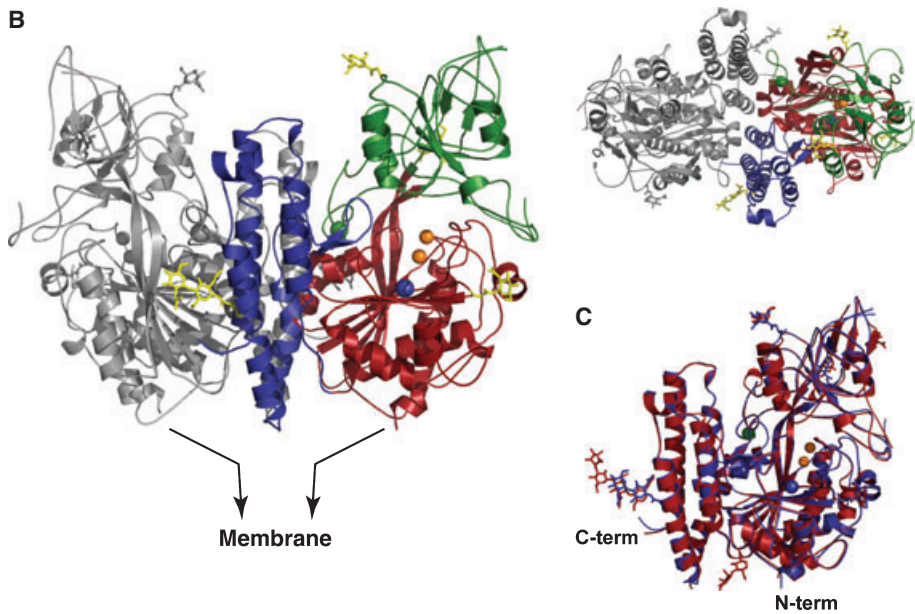
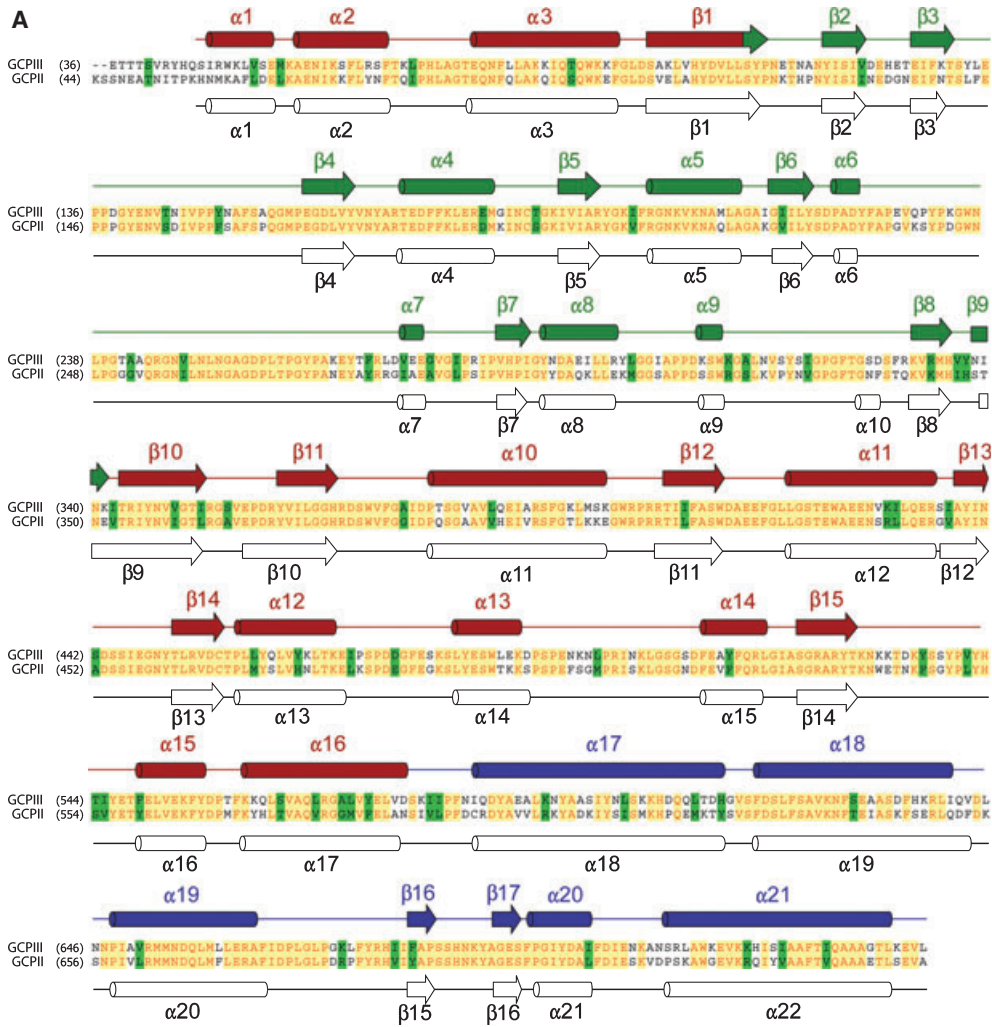
density maps of the rhGCPIII/QA complex from the X-ray data collected at an energy corresponding to the Zn²⁺ absorption edge (Fig. 2A). The combined results from both experiments unequivocally demonstrate that the bimetallic active site of GCPIII is indeed occupied by Zn²⁺ ions and that the occupancy of at least one Zn²⁺ ion is only partial.

In subsequent refinement steps, the strong difference peaks observed in the active site were modeled as Zn²⁺ ions, and their approximate occupancies were determined (by careful analysis of the B-factors of metal ions and surrounding residues, as well as difference electron density peaks) to be in the range 0.80–0.95 and 0.45–0.80 for Zn1 and Zn2, respectively.

Both the topology and identity of the Zn²⁺ coordination sphere in GCPIII are almost identical to those observed for GCPII [27]. In GCPIII, the Zn1 cation is coordinated by Asp377 (Oδ1; 2.0 Å; where values in parentheses describe the ranges of coordination distances observed for the four GCPIII structures), His543 (Nε2; 2.0–2.1 Å) and Glu415 (Oε1 and Oε2; 2.4–2.5 Å and 1.9–2.3 Å, respectively). The co-catalytic ion, Zn2, is coordinated by Asp377 (Oδ2; 2.0 Å), His367 (Nε2; 2.0–2.2 Å) and Asp443 (Oδ1 and Oδ2; 2.0–2.3 Å and 2.3–2.6 Å, respectively). The coordination sphere of the active site Zn²⁺ ions is complemented by a bridging hydroxide anion (or a water molecule) placed somewhat asymmetrically in between the two metal ions (Zn1...O...Zn2, 2.0–2.3 Å and 2.1–2.4 Å, respectively; Fig. 2B). Moreover, a second water molecule contributes to the Zn2 coordination (1.9–2.2 Å) in all of the GCPIII structures that were solved (Fig. 2B).

It should be noted that the distance between the active site Zn²⁺ ions varies depending on the type of ligand present in the substrate-binding cavity. In the ‘pseudo-unliganded’ structure and in the rhGCPIII/Glu complex (the reaction product), the Zn1...Zn2 distance is 3.7 Å. However, when a moiety mimicking the transition state of the reaction (such as the phosphinate group of EPE or the sulfate moiety of Mops) coordinates zinc ions, the distance increases to 3.9 Å, with a concomitant subtle reorganization of the active site architecture. Such variability is considered to be important during the catalytic cycle of binuclear hydrolases and has been observed previously in reported GCPII structures [27,34].

Because the occupancy of the Zn2 site in the rhGCPIII/Glu complex is 0.7, it was possible to build two alternative models of the active site residues and the S1 pocket. The side chain of Asp443, which coordinates the Zn2 ion in a monodentate/bidentate mode, is rotated by approximately 110° towards the position



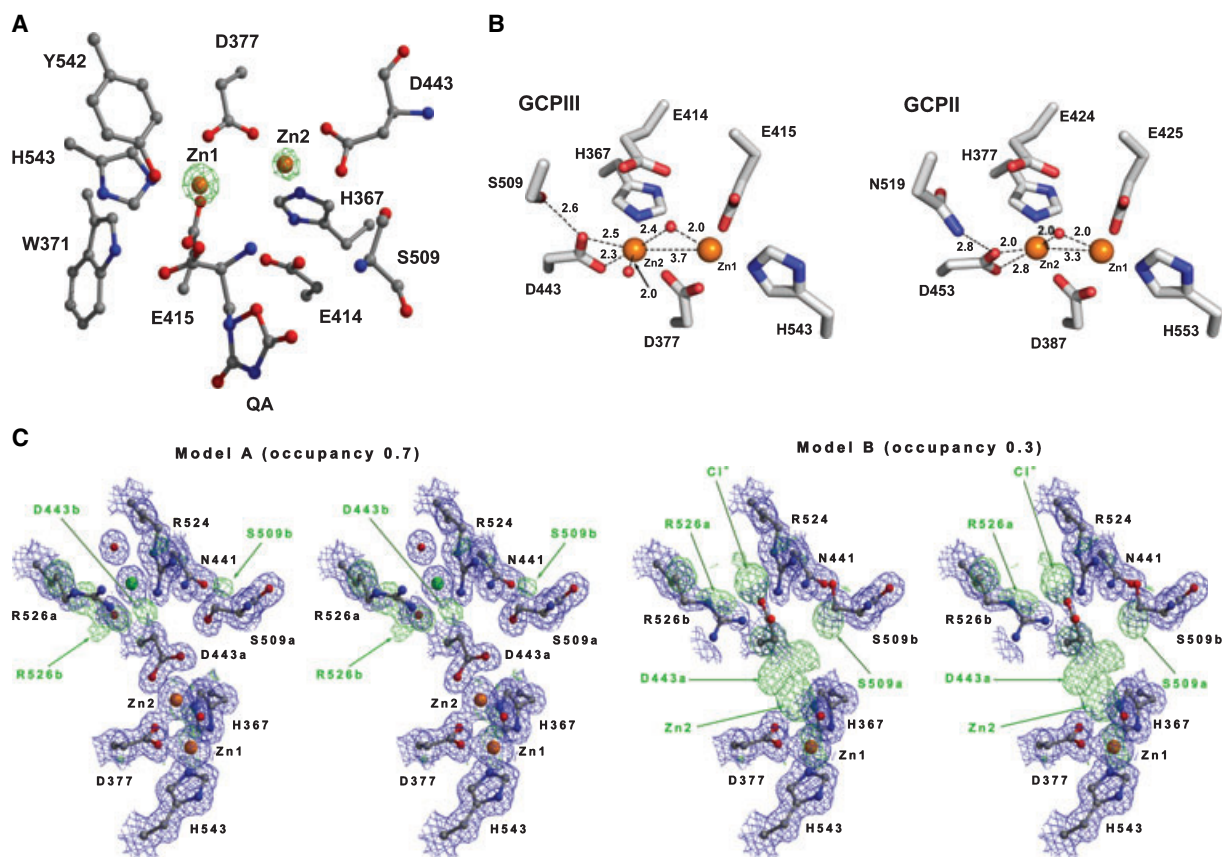


Fig. 2. The binuclear Zn^{2+} center. (A) The anomalous $F_o - F_c$ peaks (green) from the rhGCP1III/QA (PDB code 3FEE) complex contoured at the 33σ level. The residues in the vicinity of the bimetallic center are in ball-and-stick representation with carbon, oxygen and nitrogen atoms colored gray, red and blue, respectively. The Zn^{2+} ions are shown as orange spheres. The picture was generated using MOLSCRIPT [49] and BOBSCRIPT [50] and rendered with POVray (www.povray.org). (B) Comparison of Zn^{2+} coordination spheres for GCP1III (rhGCP1III/QA complex; PDB code 3FEE) and GCP1II (rhGCP1II/QA complex; PDB code 2OR4). The residues around zinc ions (orange spheres) are in stick representation; selected interatomic contacts are shown as dashed lines, together with the corresponding distances (\AA). (C) Alternate conformations of the active site Asp443 and accompanying rearrangements in the S1 pocket of the GCP1III/Glu complex (PDB code 3FF3). Model A (occupancy 0.7): Asp443 coordinates the $Zn2$ ion, and the side chains of Arg526 and Ser509 are in conformation 'A'. Model B (occupancy 0.3): with the $Zn2$ ion absent, the Asp443 side chain rotates by 110° , and this alternate conformation is stabilized by hydrogen bonds with the side chains of Arg524, Asn441 and Arg526b. Concomitantly, the chloride anion is 'pushed out' from the S1 site. Atoms of residues in ball-and-stick representation are colored gray (carbon), blue (nitrogen) and red (oxygen). Water molecules are shown as red spheres, and the ions are represented by green (chloride) and orange (zinc) spheres. The $F_o - F_c$ electron density map is contoured at the 3σ level (green) and the $2F_o - F_c$ electron density map at the 1σ level (blue). The green captions point to the $F_o - F_c$ electron density peaks corresponding to the alternate (unmodeled) conformations of a given residue. The picture was generated using MOLSCRIPT [49] and BOBSCRIPT [50], and rendered with POVray.

Fig. 1. Overall structure of GCP1III. (A) Structure-based alignment of GCP1III and GCP1II extracellular domains. The secondary structure motifs were analyzed with IMOLTALK [47] using the rhGCP1III/EPE (PDB code 3FED) and rhGCP1II/EPE (PDB code 3BI0) structural data [29]. Individual segments of GCP1III are colored according to domain organization: red, protease domain; green, apical domain; blue, helical domain. (B) Front and top views of the GCP1III dimer. One monomer is colored according to domain organization, as in (A), whereas the second monomer is shown in gray. Orange spheres represent the zinc ions, the blue sphere represents the Cl^- ion, and the Ca^{2+} ion is shown as a green sphere. N-glycosylations are shown in stick-representation (yellow). The 'MEMBRANE' arrows symbolically depict how the full-length protein N-terminal sequence continues to be anchored in the membrane. (C) Superposition of rhGCP1III/EPE (blue; PDB code 3FED) and rhGCP1II/EPE (red; PDB code 3BI0) complexes. The rmsd for the equivalent $C\alpha$ atoms in the two structures is 1.0 \AA . The ion representation is the same as in (B). Generated using PYMOL [48].

of the S1-bound chloride anion and ‘pushes’ the Cl⁻ out of the bottom of the S1 pocket (the occupancy of the Cl⁻ in this structure is 0.7). The alternate conformation of the Asp443 side chain (D443b with an occupancy of 0.3) is stabilized by interactions with the side chains of Arg524, Asn441 and Arg526 (Fig. 2C). It is plausible that the observed flexibility of Asp443, which is not found in any of the GCPII structures [27–30,32], is linked to the variations in amino acids surrounding the GCPIII active site, in particular to the presence of Ser509 in place of Asn519 in GCPII. Given the apparent steric freedom of Ser509, as revealed by the existence of two alternate conformations of its side chain, stabilization of the Asp443 position as a result of a

hydrogen bond to the Ser509 hydroxyl group might be weakened. Decreased stabilization of this hydrogen bond could result in loosened coordination of Zn2 and a propensity for Asp443 to adopt a stable alternate conformation when the Zn2 ion is absent (Fig. 2B,C).

The S1 pocket and the ‘entrance lid’

Out of the four GCPIII structures reported in the present study, only the rhGCPIII/EPE complex features the S1 specificity pocket occupied by the P1 moiety of the inhibitor. The S1 pocket is primarily defined by Arg526, Arg524, Arg453, Glu447, Gly508, Ser509 and Ser538 (Fig. 3A), with the positively-charged side

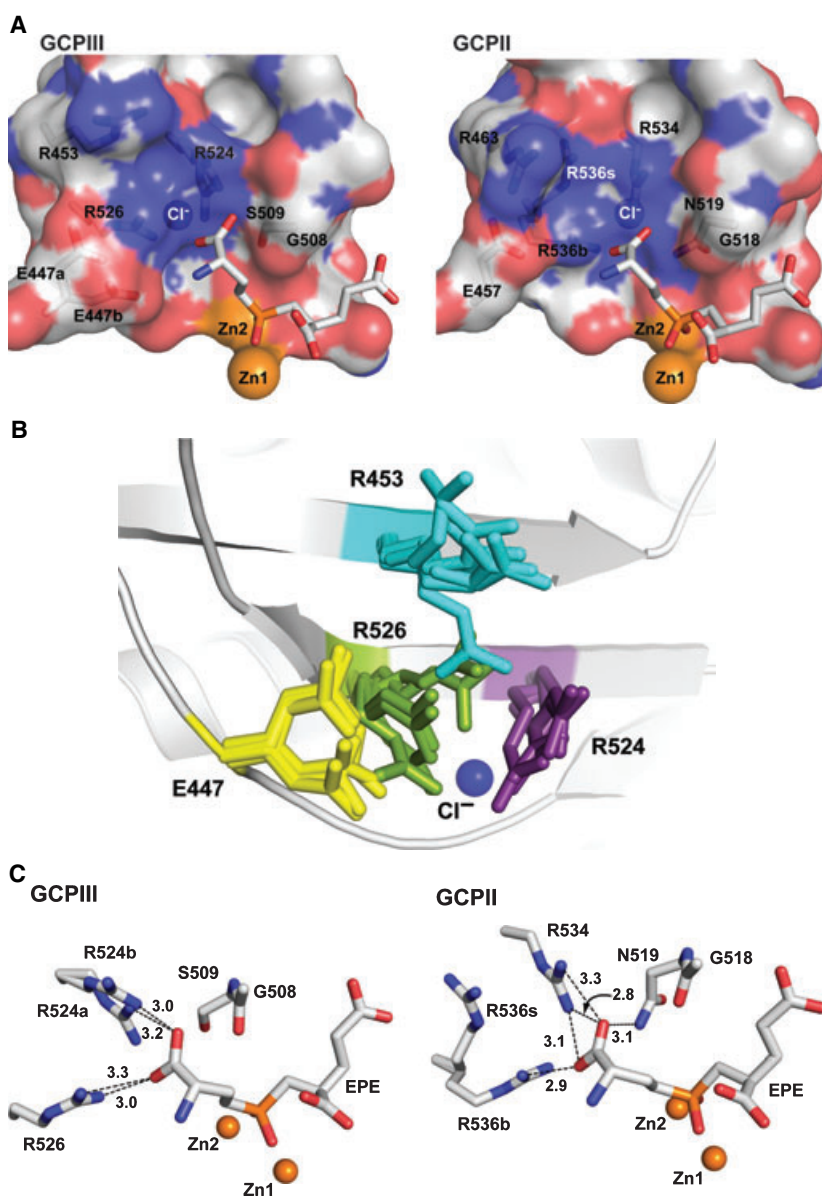


Fig. 3. Enzyme–inhibitor interactions and the architecture of the S1 pocket. (A) A semi-transparent surface representation of the S1 pocket in the rhGCPIII/EPE (PDB code 3FED) and rhGCPII/EPE (PDB code 3B10) complexes. The dissected S1 pockets are shown in semi-transparent surface representation, whereas the EPE ligands are in stick representation. Atoms are colored blue (chloride ion), orange (zinc ions), gray (carbon), blue (nitrogen), red (oxygen) and orange (phosphorus). The GCPII R536b and R536s residues refer to the Arg536 binding and stacking conformations, respectively, as described previously [29]. (B) The conformational variability of the GCPIII S1 site. All four GCPIII structures (PDB codes 3FED, 3FF3, 3FEE and 3FEC) are superposed on the corresponding C α atoms to show the flexibility of Glu447 (yellow), Arg526 (green), Arg453 (cyan) and Arg524 (purple). The chloride ion, located near the S1 site, is represented by a blue sphere. (C) The hydrogen bonding interactions between the active site bound inhibitor (EPE) and the S1 residues of GCPIII (rhGCPIII/EPE complex, PDB code 3FED) and GCPII (rhGCPII/EPE complex, PDB code 3B10) are shown as dashed lines, together with the interatomic distances (Å). The coloring scheme is as used in (A) (the chloride ion is not depicted).

chains of Arg526, Arg524 and Arg453 forming an 'arginine patch' that is implicated in the preference of GCPIII for negatively-charged P1 residues [25]. This cluster of positively-charged residues is stabilized by the presence of a chloride anion that is coordinated in a distorted octahedral manner by the Arg524, Arg570 and Asn441 side chains; an Asp443 main chain amide; one or two water molecules; and, in the rhGCPIII/QA complex, the side chain of Arg526. A comparison of the four GCPIII structures reveals high conformational variability in the S1 site (Fig. 3B), including multiple conformations of the S1 arginines, as well as changes in the immediate surroundings of the chloride anion. By contrast to the GCPII S1 site architecture, multiple conformations are observed for the side chains of Glu447 and Arg524 of GCPIII and, compared to GCPII, Arg453 and Arg526, also exhibit increased conformational flexibility. The structural variability of the S1 site in GCPIII significantly affects the charge distribution on the surface of the active site pocket compared to GCPII (Fig. 3A).

The enzyme–inhibitor interactions in the S1 pocket of the rhGCPIII/EPE complex are represented by four water-mediated contacts and, most importantly, direct interactions between the P1 carboxylic group of the inhibitor and guanidinium moieties of Arg524 (3.2 Å for conformation A and 3.0 Å for conformation B) and Arg526 (3.0 Å and 3.3 Å; Fig. 3C). In GCPII, the P1 carboxylic group is additionally hydrogen bonded to Asn519 but, in GCPIII, this interaction is absent as a result of the Asn519 to Ser509 change. The high B-factors of the P1 part of the inhibitor, as well as the adjacent S1 residues of GCPIII (compared to the lower B-factors observed for the P1' fragment and the S1' pocket), suggest that the enzyme–inhibitor interactions in the S1 pocket are somewhat weaker than in the S1' pocket and probably vary with slight modifications of the P1 moieties. These findings mirror the observations made previously for GCPII [29].

Adjacent to the S1 pocket, a flexible loop spanning residues Trp541 to Gly548 ('entrance lid') was observed to adopt either an 'open' or 'closed' conformation in GCPII complexes [29]. Stabilization of the 'closed' conformation is likely to be associated with the occupancy of the S1 pocket by a ligand and the 'open–close' transition exploits the hinges on the two sides of the lid made up of Asn540/Trp541 and Gly548 (GCPII numbering). In the GCPIII complexes described here, the 'entrance lid' is invariably in the 'open' conformation, even though the active site is always occupied by a ligand molecule, at least partially (Fig. 4). One of the reasons for the apparent preference of the lid to adopt the 'open' conformation in

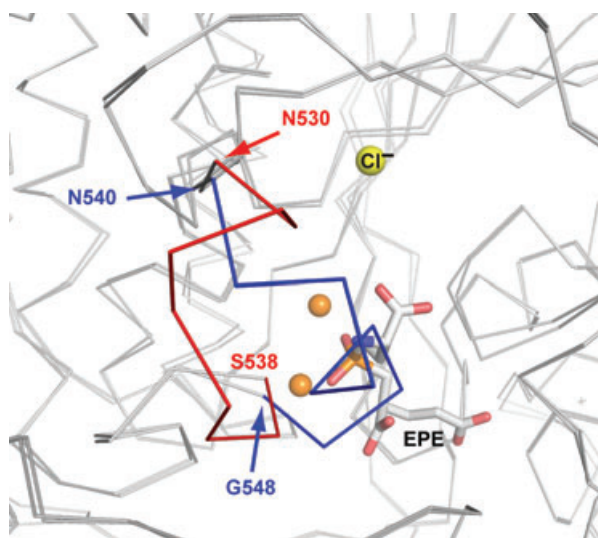


Fig. 4. Comparison of the 'entrance lid' conformations in GCPIII and GCPII. The GCPII and GCPIII complexes with EPE (PDB codes 3BI0 and 3FED, respectively) were superposed based on equivalent C α atoms. The C α traces for both proteins are colored gray and the 'entrance lids' are colored red (amino acids Asn530–Ser538) and blue (amino acids Asn540–Gly548) for GCPIII and GCPII, respectively. Note that, in GCPII, the 'entrance lid' accommodates a 'closed' conformation upon EPE binding, but such a change is not observed in GCPIII, in which the 'entrance lid' is always found in 'open' conformation. This difference is likely a result of the replacement of Gly548 (GCPII) by the less flexible Ser538 (GCPIII). The orange spheres represent zinc ions.

GCPIII might be a result of the Gly548 at the C-terminus of the lid in GCPII being replaced by Ser538 in GCPIII, thus decreasing the flexibility of this hinge. Out of the GCPII orthologues identified, the Gly548 is only present in human, chimp and gorilla, whereas the position is occupied by a serine residue (as observed in GCPIII) in other species, such as in orangutan and macaque. In this respect, it is interesting to note that the Ramachandran angles for the Gly548 residue of GCPII are highly unfavorable for any L-amino acid.

The S1' pocket and the 'glutamate sensor'

The S1' pocket, the pharmacophore pocket of GCPIII, is shaped by residues Phe199, Arg200, Asn247, Glu414, Gly417, Leu418, Gly508, Tyr542, Lys689 and Tyr690. The specificity of GCPIII towards the P1' glutamate (or glutamate-like moieties) is determined by a combination of ionic and polar interactions (Fig. 5). In all complexes, the C-terminal α -carboxylate is recognized by Arg200 through an ion pair interaction (2.8–2.9 Å for the N η 1 atom and 3.2–3.5 Å for the N η 2 atom of the guanidinium group; where values in parentheses describe the ranges of coordination dis-

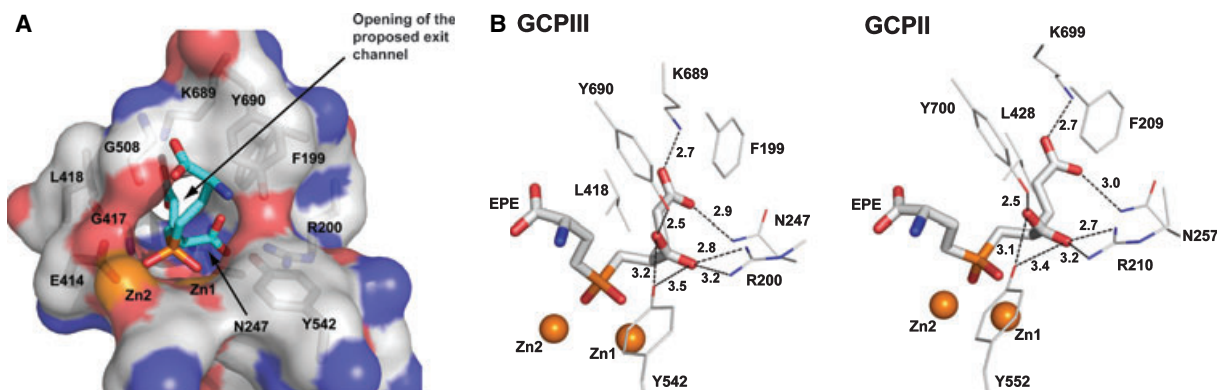


Fig. 5. Enzyme–inhibitor interactions and the architecture of the S1' pocket. (A) The residues shaping the GCPIII S1' pocket (PDB code 3FED) are shown in stick representation accompanied by a semi-transparent surface, whereas the active site bound ligand (EPE) is in stick representation. The Zn²⁺ ions are colored orange. The opening of the proposed exit channel, as suggested for GCPII in previous studies [27], is depicted. (B) Interactions between the active site bound inhibitor EPE (sticks) and the GCPIII and GCPII (PDB codes 3FED and 3BI0, respectively). S1' residues (lines) are shown as dashed lines, together with interatomic distances (Å). The Zn²⁺ ions are shown as orange spheres.

tances observed for four GCPIII structures) and via two hydrogen bonds with the OH groups of Tyr542 (3.1–3.2 Å) and Tyr690 (2.5–2.7 Å, a part of the 'glutamate sensor'; see below). The side chain γ -carboxylate group of the substrate forms a strong salt bridge with Lys689 (2.4–2.9 Å), and further interacts with the side chain amide of Asn247 (2.7–2.9 Å). In the case of the S1'-bound quisqualate, in which the γ -carboxylate of glutamate is replaced by the 1,2,4-oxadiazolidine ring, two additional polar interactions involve hydrogen bonds between the exocyclic oxygen and the Gly508 main chain amide (2.8 Å) and the Ser507 hydroxyl group (3.1 Å). These two added polar contacts, together with more extensive nonpolar interactions involving Phe199 and Leu418, are likely to be responsible for the approximately three orders of magnitude higher affinity compared to glutamate (Table 1). Furthermore, it is interesting to note that the architecture of the S1' site is mostly unchanged upon QA binding. These findings contrast with the adjustments necessary to accommodate QA in the S1' pocket of GCPII [28] and suggest that the pharmacophore pocket of GCPIII might be better-optimized for the binding of glutamate biosteres, as reflected by the four-fold higher affinity of QA for GCPIII versus GCPII (Table 1).

The free amino group in both the rhGCPIII/Glu and rhGCPIII/QA complexes interacts with the Gly508 main chain carbonyl (2.9 Å), γ -carboxylate of Glu414 (2.6–2.7 Å and 3.3–3.5 Å), the active site-bound hydroxide anion/water molecule (2.8–3.0 Å) and a water molecule that is in turn hydrogen bonded to the OH group of Tyr542. The phosphinate group of EPE (and the sulfate group of Mops), which mimics

the tetrahedral transition state of the reaction [31], coordinates the active site Zn²⁺ ions with interatomic distances of 1.9 Å (O1...Zn1) and 2.1 Å (O2...Zn2). Additionally, a network of hydrogen bonding interactions in the vicinity of the bimetallic active site involves the phosphinate/sulfate (in the rhGCPIII/EPE and rhGCPIII/'pseudo-unliganded' structures, respectively) moiety and the side chains of Glu414, Asp443, His367, Asp377, His543 and Tyr542.

The GCPIII flexible 'glutamate sensor' encompasses amino acids Ile681 to Ser694 and forms the bottom of the S1' pocket. As a result of (at least partial) occupancy of the S1' pocket by the glutamate or glutamate-like moiety, this segment adopts a closed conformation in all the GCPIII structures presented. However, in the rhGCPIII/'pseudo-unliganded' structure, the closed conformation is modeled at only 0.4 occupancy, which corresponds to the occupancy of the S1'-bound glutamate. In the remaining instances, the fragment could not be modeled because of disorder that was attributable to a multitude of open conformations. Interestingly, the apparent withdrawal (i.e. opening) of the 'glutamate sensor' from the S1' pocket is associated with a relocation of the adjacent α -helix (residues Asn168-Ile190) of approximately 2.5 Å (Fig. S1).

Discussion

In the present study, we report four high resolution structures of complexes of the extracellular part of human GCPIII and small molecule ligands. The overall fold of GCPIII is virtually invariant in all four

structures, with the rmsd between the corresponding C α atoms reaching a maximum of 0.5 Å (for the rhGCPIII/QA and rhGCPIII/‘pseudo-unliganded’ complexes). The majority of the protein residues, as well as the active site-bound ligands (with the notable exception of L-Glu and Mops partially occupying the active site in the rhGCPIII/‘pseudo-unliganded’ structure), are well defined in the electron density peaks (Fig. S2). The first ten N-terminal residues of the GCPIII ectodomain and a short fragment around Tyr133 (one to four residues) are missing from the structure. The nature of Asp327 (part of a loop on the surface of the apical domain), which is flanked by two serine residues in GCPIII, is also intriguing. Whereas the electron density of both serines is of excellent quality, the density for Asp327 is totally absent (Fig. S3). It may be of interest that this Ser-Asp-Ser motif is conserved in the GCPIII orthologs in the great apes (orangutan, chimp and gorilla), whereas it is variable in the remaining species studied (such as macaque, mouse and rat). Ramachandran analysis of the final models classifies all residues but two, Lys197 and Asn168 (in the GCPIII/‘pseudo-unliganded’ complex only), as having either favorable or allowed conformations. Despite falling into the disallowed region of the Ramachandran plot, all atoms of Lys197 and Asn168 have a well defined electron density. It is interesting to note that unfavorable backbone angles were also observed for Lys207 in GCPII, which is equivalent to Lys197 of GCPIII [27,28].

Concurrent analysis of the GCPIII structures presented here and the corresponding complexes of human GCPII reported previously [27–29] allows for a direct comparison between the two enzymes and helps to define features associated with similarities/differences in their physiological and biochemical properties. The high degree of structural similarity between human GCPII and GCPIII is apparent from the equivalent domain organization and comparable topology (Fig. 1C). Nevertheless, a few differences between both enzymes exist, including the surface distribution of electrostatic potentials, which reflects the distinct theoretical pI values of 6.4 and 8.1 for GCPII and GCPIII, respectively (Fig. S4). Based on structural homology with the receptor protein TfR [26], it is reasonable to suggest that the variability of the GCPIII/GCPII surfaces could be a major determinant in many physiological processes, such as interactions with hypothetical protein partners/ligands.

Several common motifs have been identified in both GCPIII and GCPII, including the ‘glutarate sensor’ and the Pro-rich region [27]. Both GCPII and GCPIII display an induced-fit movement of the ‘glutarate

sensor’ upon binding of a glutamate (or glutamate-like) moiety in the S1’ pocket. In GCPIII, the opening of the ‘glutarate sensor’ is associated with a repositioning of the Asn168-Ile190 fragment (a helix-turn-strand-turn-helix motif, α 4- β 5- α 5), adjacent to the S1’ pocket of up to 2.5 Å (for C α of Met182). It is worth noting that, in the rhGCPIII/‘pseudo-unliganded’ complex, the N-terminus of this segment is flanked by Asn168, a residue with disallowed Ramachandran conformation. Such repositioning was not observed in any of the reported structures of GCPII, although the analysis of the thermal parameters of the recombinant human GCPII (rhGCPII)/phosphate complex, in which the ‘glutarate sensor’ is in open conformation, suggests a higher degree of positional freedom compared to the GCPII complexes that feature the ‘glutarate sensor’ in its closed conformation [27].

There are three sequential Pro residues at positions 136–138 of GCPIII flanked by residues with a high propensity to form a polyproline type II (PPII) helix, which is an important motif in protein–protein interactions [35]. Unlike in GCPII, in which this region is well defined in the electron density map and reveals a perfect PPII helix [27], the electron density for this segment in GCPIII is weak at best. Apart from the apparent flexibility, superposition of the corresponding regions from the GCPII/GCPIII structures reveals quite different conformations (Fig. S5). Furthermore, analysis of the amino acid sequence of GCPIII suggests that the Pro-rich region in this enzyme (residues 135–139: EPPPD) does not represent a common recognition site for SH3 domains (residue sequence XPXXP). GCPII, on the other hand, does contain such a recognition motif [27,36].

The data presented here unequivocally demonstrate that the bimetallic active site of GCPIII is occupied by two Zn²⁺ ions coordinated in a manner similar to that of GCPII [27]. However, there are several noticeable differences between the states of the Zn²⁺ sites in the two enzymes. First, despite the conserved Zn²⁺ coordination shells, there is a considerable difference in the distance between the Zn²⁺ ions: 3.7 Å versus 3.3 Å for GCPIII/L-Glu and GCPII/L-Glu, respectively. This variability stems from positional differences of the His367 and Asp443 side chains (Fig. 2B), with the flexibility of the latter likely being associated with the substitution of Asn519 in GCPII by Ser509 in GCPIII. Additionally, both ion sites are only partially occupied in GCPIII, with the catalytic Zn1 and co-catalytic Zn2 displaying respective occupancies of 0.80–0.95 and 0.45–0.80. The lower occupancy of the co-catalytic Zn2 versus the catalytic metal suggests that the former has a lower binding affinity, which is in agreement

with the binding constants reported for other binuclear proteases [34]. The lower Zn^{2+} occupancies in GCPIII (compared to GCPII) cannot be unambiguously explained and might, for example, reflect different Zn^{2+} binding affinities or simply result from different purification protocols. Almost all of the co-catalytic metalloenzymes studied display 75–90% activity with only one Zn^{2+} ion present, consistent with the theory that the catalytic metal in two-zinc metalloenzymes plays a central role in their activity [34,37]. The suggested role of the co-catalytic zinc ion is to enable productive positioning of the substrate/reaction intermediate [31,34]. In GCPII/GCPIII, there are no direct interactions between the co-catalytic Zn2 and a substrate, although Zn2 is believed to play a role in positioning the bridging water molecule away from the catalytic Glu424 and helping stabilize the transition state [31]. However, additional studies are needed to address these issues in more detail.

In each of the four GCPIII complexes reported in the present study, the S1' site is (at least partially) occupied by a glutarate fragment of a ligand/inhibitor. The pattern of GCPIII substrate/inhibitor binding is virtually identical to that of GCPII, suggesting that the S1' pockets of both proteins are optimized for glutamate binding [27,28] (Fig. 5). However, because of increased rotational freedom of the Ser509 side chain (as opposed to Asn519 in GCPII), the Ser507-Ser509 loop lining the S1' pocket appears to be more flexible in GCPIII, allowing GCPIII to accommodate bulkier inhibitor moieties without the need for additional structural adjustments. This characteristic is apparent on comparing complexes of both enzymes with QA. In the GCPII complex, Ser517-Asn519 undergoes relocation upon inhibitor binding and, in addition, a rotation of the Asn257 side chain is necessary to accommodate the bulky oxodiazolidine ring. These observations are in line with the four-fold higher potency of QA towards GCPIII (compared to GCPII) and could be exploited for the design of GCPIII-specific inhibitors.

Conclusions

In the present study, we report the first high resolution structures of human GCPIII and compare them in detail with the equivalent structures of human GCPII. These four structures provide information on the overall architecture of the enzyme and detail enzyme–ligand interactions in the GCPIII specificity pocket. It is quite evident that, despite high homology between GCPIII and GCPII, several motifs/features located in or around the active sites of these enzymes differ. They

include the 'entrance lid', Pro-rich region, the loop regions lining the S1' site, or the occupancies of Zn^{2+} sites. All these elements will have to be considered in the future development of any potent inhibitors of glutamate carboxypeptidase activity. Finally, the information provided in the present study should prove to be essential for the structurally-aided design of GCPIII-specific therapeutics and ligands, as well as in the investigation of the diverse biological functions of GCPIII and GCPII.

Experimental procedures

rhGCPIII and rhGCPII expression and purification

The extracellular portions of human GCPII and GCPIII (rhGCPII and rhGCPIII; amino acids 44–750 and 36–740, respectively), were expressed and purified as described previously [25,38]. Briefly, rhGCPIII was heterologously over-expressed in *Drosophila* Schneider's S2 cells. The protein was purified from the conditioned medium by two ion-exchange chromatography steps (QAE-Sephadex A50 in batch, Source 15S column; GE Healthcare, Little Chalfont, UK) followed by size-exclusion (Superdex HR200 column 16/60; GE Healthcare) chromatography. The purified rhGCPIII was dialyzed against 20 mM Mops and 20 mM NaCl (pH 7.4) and concentrated to $12 \text{ mg}\cdot\text{mL}^{-1}$ ($130 \mu\text{M}$) or $125 \mu\text{g}\cdot\text{mL}^{-1}$ ($1.4 \mu\text{M}$) for the structural and kinetic experiments, respectively. For crystallization, the final protein was > 98% pure as determined by silver stained SDS/PAGE. The stock solution was frozen at $-80 \text{ }^\circ\text{C}$ until further use.

Inhibitors

A pure preparation (99%, assayed by TLC) of QA was purchased from Fluka (Sigma–Aldrich, St Louis, MO, USA). The stock solution was prepared by dissolving 1 mg of QA in 66 μL of 100 mM NaOH (80 mM final concentration). NAAG was purchased from Sigma–Aldrich and dissolved in distilled water to a final concentration of 20 mM. The synthesis of EPE has been described previously [29]. For crystallization experiments, EPE was dissolved in distilled water to a final concentration of 50 mM.

Crystallization, data collection and processing

Initial crystallization experiments were carried out for the complex of rhGCPIII and EPE with the aid of a Phoenix crystallization robot (Art Robbins Instruments, Sunnyvale, CA, USA) and various commercial crystallization screens at 293 °K. Screening was performed with a 20 : 1 molar ratio of inhibitor and enzyme ($12 \text{ mg}\cdot\text{mL}^{-1}$) in the presence of 20 mM Mops (pH 7.4) and 20 mM NaCl in a sitting drop

Table 2. Data collection and refinement statistics. Values in parentheses correspond to the highest resolution shells.

	rhGCPIII/EPE	rhGCPIII/Glu	rhGCPIII/QA	rhGCPIII/'pseudo-unliganded'
PDB code	3FED	3FF3	3FEE	3FEC
Data collection statistics				
Wavelength (Å)	1.0000	1.0000	1.2759	1.0000
Temperature (°K)	100			
Space group	C2			
Unit-cell parameters: a, b, c (Å); β (°)	122.7, 104.1, 77.6; 108.2	122.5, 104.1, 77.6; 108.0	123.0, 103.7, 77.6; 108.3	122.8, 104.3, 78.0; 107.7
Resolution limits (Å)	30.0–1.29 (1.34–1.29)	20.0–1.37 (1.42–1.37)	50.0–1.56 (1.62–1.56)	20.0–1.49 (1.54–1.49)
Number of unique reflections	227958 (18560)	189722 (17742)	130199 (12705)	148978 (14188)
Redundancy	6.6 (3.0)	4.5 (2.8)	3.6 (3.5)	4.9 (3.4)
Completeness (%)	97.8 (79.8)	98.0 (92.0)	99.2 (97.0)	97.8 (93.6)
I/σ (I)	16.1 (1.9)	16.5 (2.0)	21.8 (4.9)	15.1 (2.0)
R_{merge}	0.092 (0.469)	0.077 (0.498)	0.049 (0.261)	0.079 (0.525)
Refinement statistics				
Resolution limits (Å)	25.0–1.29 (1.33–1.29)	25.0–1.37 (1.41–1.37)	25.0–1.56 (1.60–1.56)	25.0–1.49 (1.53–1.49)
Total number of reflections	225644 (14595)	185390 (12878)	128862 (9412)	145908 (9720)
Number of reflections in working set	223352 (14444)	181584 (12632)	127549 (9319)	142925 (9562)
Number of reflections in test set	2292 (151)	3806 (246)	1313 (93)	2983 (188)
R -factor	0.131 (0.220)	0.133 (0.236)	0.149 (0.217)	0.159 (0.218)
Free- R	0.147 (0.219)	0.154 (0.256)	0.184 (0.233)	0.183 (0.245)
Total number of nonhydrogen atoms	6784	6974	6647	6736
Number of nonhydrogen protein atoms	5903	5929	5806	5949
Number of ions	4	4	4	4
Number of water molecules	861	994	828	752
Average B-factor (Å ²)				
Protein atoms	16.4	11.9	15.8	22.8
Water molecules	31.9	28.9	29.9	36.5
Ligand atoms	16.0	7.9	13.3	28.6 / 23.0 (Mops/Glu)
rmsd				
Bond lengths (Å)	0.017	0.020	0.019	0.020
Bond angles (°)	1.83	1.84	1.86	1.88
Planarity (Å)	0.014	0.013	0.012	0.013
Chiral centers (Å ³)	0.125	0.133	0.132	0.140
Ramachandran plot (%) ^a				
Most favored	90.8	90.3	90.2	90.1
Additionally allowed	8.5	9.0	9.1	9.2
Generously allowed	0.5	0.5	0.5	0.35
Disallowed	0.2	0.2	0.2	0.35
Missing residues	133–135, 327	133–135, 327	133, 327, 531–533	133–136, 327

^a Calculated with PROCHECK [44].

vapor diffusion setup. Well-diffracting crystals were obtained from a reservoir solution containing 0.1 M Hepes-Na (pH 7.5), 10% (w/v) PEG 6000 (Carl Roth GmbH, Karlsruhe, Germany) and 5% (v/v) MPD. Similar conditions were subsequently adopted for the crystallization of all complexes described in the present study. To grow crys-

tals used in the diffraction experiments, a solution of rhGCPIII (8 mg·mL⁻¹) was mixed in a 10 : 1 ratio with stock solutions (see above) of NAAG (20 mM), quisqualate (80 mM) or EPE (50 mM). All crystals were grown at 293 °K by vapor diffusion in hanging drops formed by equal volumes of the protein and reservoir solutions.

Crystals belonging to the C2 space group typically appeared within 2 days. Prior to freezing, crystals were briefly soaked in reservoir solutions supplemented with 20% (v/v) glycerol. Each of the four datasets was collected from a single crystal at 100 °K using synchrotron radiation at the SER-CAT sector 22 beamlines of the Advanced Photon Source (Argonne, IL, USA) equipped with MAR225 or MAR300 CCD detectors. Data were integrated and scaled using the software package HKL2000 [39].

Structure solution and refinement

The structure of the rhGCPIII/EPE complex was solved by the molecular replacement method using the software PHASER [40], with the previously reported structure of the rhGCPII/QA complex [Protein data Bank (PDB) accession code 2OR4] being employed as the search model [28]. The solution was unambiguous with a final Z-score of 56.3 and a log-likelihood gain of 2604. The remaining three (isomorphous) structures were determined by Fourier difference methods using the rhGCPIII/EPE complex as a starting model. For each structure, iterative cycles of model building and structure refinement were carried out using the software X-FIT [41], COOT [42] and REFMAC 5.0 [43]. Models were initially refined at a resolution of 2.3 Å, and resolution limits were gradually extended to the resolution limits of the data. In the final steps, structural refinement utilizing the anisotropic model for the atomic displacement parameters was used in the case of the rhGCPIII/EPE and rhGCPIII/Glu complexes, whereas the rhGCPIII/QA and rhGCPIII/‘pseudo-unliganded’ complexes were refined using the isotropic model. The stereochemical quality of the refined structures was analyzed using the software PROCHECK [44] and MOLPROBILY [45], and the final statistics are summarized in Table 2.

X-ray fluorescence scans and anomalous maps

To determine the nature of the metals occupying the bimetallic active site of GCPII, we performed X-ray fluorescence scan analysis around the K-edge of Zn²⁺ ions using a single crystal of the rhGCPIII/EPE complex. The resulting absorption spectrum confirmed the presence of Zn²⁺ ions in the sample studied (data not shown). To verify and bolster the fluorescence scan results, we collected a complete dataset of diffraction intensities from a single crystal of the rhGCPIII/QA complex at the energy corresponding to the Zn²⁺ absorption edge ($\lambda = 1.2759$ Å). Calculation of the anomalous electron density maps revealed only two anomalous peaks stronger than 5 σ , and the positions of these peaks matched the metal sites in GCPIII. The heights of these peaks, 70 σ and 50 σ , corresponding to Zn1 and Zn2, respectively, indicated that Zn²⁺ ions indeed occupy the active site of GCPIII, and that the occupancy of at least one site is partial.

Determination of inhibition constants

Solutions of rhGCPIII (75 ng·mL⁻¹/830 pM) or rhGCPII (30 ng·mL⁻¹/330 pM) were pre-incubated with varying inhibitor concentrations in 20 mM Mops and 20 mM NaCl (pH 7.4) for 10 min at 37 °C in a final volume of 180 μ L. A radiometric assay using [³H]NAAG (radiolabeled on the terminal glutamate) was used to measure the activities, as described previously [25]. The IC₅₀ values were determined from the plots of v_i/v_0 (i.e. the ratio of individual reaction rates to the rate of the uninhibited reaction) against the inhibitor concentration using GRAFIT, version 5.0.4 (Erithacus Software Ltd, Horley, UK). These were then used to calculate the K_i values using Morrison’s formula for competitive inhibitors [46].

Acknowledgements

We thank Takashi Tsukamoto and Pavel Majer for the generous gift of EPE, Jana Starkova for excellent technical assistance, Zbyszek Dauter for assistance with the X-ray experiments, and Hillary Hoffman for corrections to the language. Diffraction data were collected at the South-East Regional Collaborative Access Team (SER-CAT) beamline 22-ID at the Advanced Photon Source, Argonne National Laboratory. The use of the Advanced Photon Source was supported by the US Department of Energy, Office of Science, Office of Basic Energy Sciences, under Contract No. W-31-109-Eng38. This project was supported in part by the Intramural Research Program of the NIH, National Cancer Institute, Center for Cancer Research (J.L. and C.B.). J.K. and K.H. were supported in part by the Ministry of Education of the Czech Republic (Research Centre for New Antivirals and Antineoplastics, 1M0508).

References

- 1 Lambert LA & Mitchell SL (2007) Molecular evolution of the transferrin receptor/glutamate carboxypeptidase II family. *J Mol Evol* **64**, 113–128.
- 2 Rawlings ND, Morton FR, Kok CY, Kong J & Barrett AJ (2008) MEROPS: the peptidase database. *Nucleic Acids Res* **36**, D320–D325.
- 3 Bzdega T, Crowe SL, Ramadan ER, Sciarretta KH, Olszewski RT, Ojeifo OA, Rafalski VA, Wroblewska B & Neale JH (2004) The cloning and characterization of a second brain enzyme with NAAG peptidase activity. *J Neurochem* **89**, 627–635.
- 4 Pangalos MN, Neefs JM, Somers M, Verhasselt P, Bekkers M, van der Helm L, Fraiponts E, Ashton D & Gordon RD (1999) Isolation and expression of novel human glutamate carboxypeptidases with N-acetylated

- alpha-linked acidic dipeptidase and dipeptidyl peptidase IV activity. *J Biol Chem* **274**, 8470–8483.
- 5 Carter RE, Feldman AR & Coyle JT (1996) Prostate-specific membrane antigen is a hydrolase with substrate and pharmacologic characteristics of a neuropeptidase. *Proc Natl Acad Sci USA* **93**, 749–753.
 - 6 Heston WD (1997) Characterization and glutamyl preferring carboxypeptidase function of prostate specific membrane antigen: a novel folate hydrolase. *Urology* **49**, 104–112.
 - 7 Rovenska M, Hlouchova K, Sacha P, Mlcochova P, Horak V, Zamecnik J, Barinka C & Konvalinka J (2008) Tissue expression and enzymologic characterization of human prostate specific membrane antigen and its rat and pig orthologs. *Prostate* **68**, 171–182.
 - 8 Sacha P, Zamecnik J, Barinka C, Hlouchova K, Vicha A, Mlcochova P, Hilgert I, Eckschlager T & Konvalinka J (2007) Expression of glutamate carboxypeptidase II in human brain. *Neuroscience* **144**, 1361–1372.
 - 9 Troyer JK, Beckett ML & Wright GL Jr (1995) Detection and characterization of the prostate-specific membrane antigen (PSMA) in tissue extracts and body fluids. *Int J Cancer* **62**, 552–558.
 - 10 Robinson MB, Blakely RD, Couto R & Coyle JT (1987) Hydrolysis of the brain dipeptide *N*-acetyl-L-aspartyl-L-glutamate. Identification and characterization of a novel *N*-acetylated alpha-linked acidic dipeptidase activity from rat brain. *J Biol Chem* **262**, 14498–14506.
 - 11 Neale JH, Olszewski RT, Gehl LM, Wroblewska B & Bzdega T (2005) The neurotransmitter *N*-acetylaspartylglutamate in models of pain, ALS, diabetic neuropathy, CNS injury and schizophrenia. *Trends Pharmacol Sci* **26**, 477–484.
 - 12 Bostwick DG, Pacelli A, Blute M, Roche P & Murphy GP (1998) Prostate specific membrane antigen expression in prostatic intraepithelial neoplasia and adenocarcinoma: a study of 184 cases. *Cancer* **82**, 2256–2261.
 - 13 Holmes EH (2001) PSMA specific antibodies and their diagnostic and therapeutic use. *Expert Opin Investig Drugs* **10**, 511–519.
 - 14 Mease RC, Dusich CL, Foss CA, Ravert HT, Dannals RF, Seidel J, Prideaux A, Fox JJ, Sgouros G, Kozikowski AP *et al.* (2008) N-[N-[(S)-1,3-Dicarboxypropyl]carbamoyl]-4-[18F]fluorobenzyl-L-cysteine, [18F]DCFBFC: a new imaging probe for prostate cancer. *Clin Cancer Res* **14**, 3036–3043.
 - 15 Mohammed AA, Shergill IS, Vandal MT & Gujral SS (2007) ProstaScint and its role in the diagnosis of prostate cancer. *Expert Rev Mol Diagn* **7**, 345–349.
 - 16 Maresca KP, Hillier SM, Femia FJ, Keith D, Barone C, Joyal JL, Zimmerman CN, Kozikowski AP, Barrett JA, Eckelman WC *et al.* (2009) A series of halogenated heterodimeric inhibitors of prostate specific membrane antigen (PSMA) as radiolabeled probes for targeting prostate cancer. *J Med Chem* **52**, 347–357.
 - 17 Liu T, Wu LY, Choi JK & Berkman CE (2009) In vitro targeted photodynamic therapy with a pyropheophorbide – a conjugated inhibitor of prostate-specific membrane antigen. *Prostate* **69**, 585–594.
 - 18 Rajasekaran SA, Christiansen JJ, Schmid I, Oshima E, Sakamoto K, Weinstein J, Rao NP & Rajasekaran AK (2008) Prostate-specific membrane antigen associates with anaphase-promoting complex and induces chromosomal instability. *Mol Cancer Ther* **7**, 2142–2151.
 - 19 Conway RE, Petrovic N, Li Z, Heston W, Wu D & Shapiro LH (2006) Prostate-specific membrane antigen regulates angiogenesis by modulating integrin signal transduction. *Mol Cell Biol* **26**, 5310–5324.
 - 20 Rajasekaran AK, Anilkumar G & Christiansen JJ (2005) Is prostate-specific membrane antigen a multi-functional protein? *Am J Physiol Cell Physiol* **288**, C975–C981.
 - 21 Copley SD (2003) Enzymes with extra talents: moonlighting functions and catalytic promiscuity. *Curr Opin Chem Biol* **7**, 265–272.
 - 22 Todd AE, Orengo CA & Thornton JM (2001) Evolution of function in protein superfamilies, from a structural perspective. *J Mol Biol* **307**, 1113–1143.
 - 23 Bacich DJ, Ramadan E, O’Keefe DS, Bukhari N, Wegerzewska I, Ojeifo O, Olszewski R, Wrenn CC, Bzdega T, Wroblewska B *et al.* (2002) Deletion of the glutamate carboxypeptidase II gene in mice reveals a second enzyme activity that hydrolyzes *N*-acetylaspartylglutamate. *J Neurochem* **83**, 20–29.
 - 24 Tsai G, Dunham KS, Drager U, Grier A, Anderson C, Collura J & Coyle JT (2003) Early embryonic death of glutamate carboxypeptidase II (NAALADase) homozygous mutants. *Synapse* **50**, 285–292.
 - 25 Hlouchova K, Barinka C, Klusak V, Sacha P, Mlcochova P, Majer P, Rulisek L & Konvalinka J (2007) Biochemical characterization of human glutamate carboxypeptidase III. *J Neurochem* **101**, 682–696.
 - 26 Davis MI, Bennett MJ, Thomas LM & Bjorkman PJ (2005) Crystal structure of prostate-specific membrane antigen, a tumor marker and peptidase. *Proc Natl Acad Sci USA* **102**, 5981–5986.
 - 27 Mesters JR, Barinka C, Li W, Tsukamoto T, Majer P, Slusher BS, Konvalinka J & Hilgenfeld R (2006) Structure of glutamate carboxypeptidase II, a drug target in neuronal damage and prostate cancer. *EMBO J* **25**, 1375–1384.
 - 28 Barinka C, Rovenska M, Mlcochova P, Hlouchova K, Plechanovova A, Majer P, Tsukamoto T, Slusher BS, Konvalinka J & Lubkowski J (2007) Structural insight into the pharmacophore pocket of human glutamate carboxypeptidase II. *J Med Chem* **50**, 3267–3273.
 - 29 Barinka C, Hlouchova K, Rovenska M, Majer P, Dauter M, Hin N, Ko YS, Tsukamoto T, Slusher BS, Konvalinka J *et al.* (2008) Structural basis of interac-

- tions between human glutamate carboxypeptidase II and its substrate analogs. *J Mol Biol* **376**, 1438–1450.
- 30 Barinka C, Starkova J, Konvalinka J & Lubkowski J (2007) A high-resolution structure of ligand-free human glutamate carboxypeptidase II. *Acta Crystallogr Sect F Struct Biol Cryst Commun* **63**, 150–153.
- 31 Klusák V, Barinka C, Plechanovová A, Mlěochová P, Konvalinka J, Rulíšek L & Lubkowski J (2009) Reaction mechanism of glutamate carboxypeptidase II revealed by mutagenesis, X-ray crystallography and computational methods. *Biochemistry* **48**, 4126–4138.
- 32 Barinka C, Byun Y, Dusich CL, Banerjee SR, Chen Y, Castanares M, Kozikowski AP, Mease RC, Pomper MG & Lubkowski J (2008) Interactions between human glutamate carboxypeptidase II and urea-based inhibitors: structural characterization. *J Med Chem* **51**, 7737–7743.
- 33 Zhou J, Neale JH, Pomper MG & Kozikowski AP (2005) NAAG peptidase inhibitors and their potential for diagnosis and therapy. *Nat Rev Drug Discov* **4**, 1015–1026.
- 34 Holz RC, Bzymek KP & Swierczek SI (2003) Co-catalytic metallopeptidases as pharmaceutical targets. *Curr Opin Chem Biol* **7**, 197–206.
- 35 Stapley BJ & Creamer TP (1999) A survey of left-handed polyproline II helices. *Protein Sci* **8**, 587–595.
- 36 Rath A, Davidson AR & Deber CM (2005) The structure of ‘unstructured’ regions in peptides and proteins: role of the polyproline II helix in protein folding and recognition. *Biopolymers* **80**, 179–185.
- 37 McCall KA, Huang C & Fierke CA (2000) Function and mechanism of zinc metalloenzymes. *J Nutr* **130**, 1437S–1446S.
- 38 Barinka C, Rinnova M, Sacha P, Rojas C, Majer P, Slusher BS & Konvalinka J (2002) Substrate specificity, inhibition and enzymological analysis of recombinant human glutamate carboxypeptidase II. *J Neurochem* **80**, 477–487.
- 39 Otwinowski Z & Minor W (1997) Processing of X-ray diffraction data collected in oscillation mode. *Methods Enzymol* **276**, 307–326.
- 40 McCoy AJ, Grosse-Kunstleve RW, Adams PD, Winn MD, Storoni LC & Read RJ (2007) Phaser crystallographic software. *J Appl Crystallogr* **40**, 658–674.
- 41 McRee DE (2008) XtalView/Xfit – a versatile program for manipulating atomic coordinates and electron density. *J Struct Biol* **125**, 156–165.
- 42 Emsley P & Cowtan K (2004) Coot: model-building tools for molecular graphics. *Acta Crystallogr D Biol Crystallogr* **60**, 2126–2132.
- 43 Murshudov GN, Vagin AA & Dodson EJ (1997) Refinement of macromolecular structures by the maximum-likelihood method. *Acta Crystallogr D Biol Crystallogr* **53**, 240–255.
- 44 Laskowski RA, McArthur MW, Moss DS & Thornton JM (1993) PROCHECK: a program to check the stereochemical quality of protein structures. *J Appl Crystallogr* **26**, 283–291.
- 45 Lovell SC, Davis IW, Arendall WB III, de Bakker PI, Word JM, Prisant MG, Richardson JS and Richardson DC (2003) Structure validation by Calpha geometry: phi, psi and Cbeta deviation. *Proteins* **50**, 437–450.
- 46 Morrison JF (1969) Kinetics of the reversible inhibition of enzyme-catalysed reactions by tight-binding inhibitors. *Biochim Biophys Acta* **185**, 269–286.
- 47 Diemand AV & Scheib H (2004) iMolTalk: an interactive, internet-based protein structure analysis server. *Nucleic Acids Res* **32**, W512–W516.
- 48 DeLano WL (2002) *The PyMOL User's Manual 2002*. DeLano Scientific, San Carlos, CA, USA.
- 49 Kraulis PJ (1991) MOLSCRIPT: a program to produce both detailed and schematic plots of protein structures. *J Appl Crystallogr* **24**, 946–950.
- 50 Esnouf RM (1999) Further additions to MolScript version 1.4, including reading and contouring of electron-density maps. *Acta Crystallogr D Biol Crystallogr* **55**, 938–940.

Supporting information

The following supplementary material is available:

Fig. S1. The effect of the ‘glutarate sensor’ (residues Ile681–Ser694) relocation on the position of the nearby α -helix (residues Asn168–Ile190) as observed in the rhGCPIII/‘pseudo-unliganded’ structure.

Fig. S2. The active site ligands of the GCPIII/‘pseudo-unliganded’ complex.

Fig. S3. The $F_o - F_c$ electron density maps for residues Gly325–Phe329 contoured at 1σ level.

Fig. S4. The electrostatic potential mapped on the molecular surfaces of GCPIII and GCPII.

Fig. S5. A comparison of the proline-rich regions in structures of GCPII and GCPIII.

This supplementary material can be found in the online article.

Please note: As a service to our authors and readers, this journal provides supporting information supplied by the authors. Such materials are peer-reviewed and may be re-organized for online delivery, but are not copy-edited or typeset. Technical support issues arising from supporting information (other than missing files) should be addressed to the authors.